JOURNAL OF CATALYSIS **162,** 349–358 (1996)
ARTICLE NO. 0292

Influence of the Nickel Reduction Degree on the Toxicity of H_2S and Thiophene over a Ni/SiO_2 Catalyst

A. Díaz,*[,1] L. M. Gandía,† J. A. Odriozola,‡ and M. Montes*[,2]

*Grupo de Ingeniería Química, Departamento de Química Aplicada, Facultad de Ciencias Químicas de San Sebastián, Universidad del País Vasco, Apdo. 1072, 28080 San Sebastián, Spain; †Departamento de Química, Universidad Pública de Navarra, Campus de Arrosadía, 31006 Pamplona, Spain; and ‡Departamento de Química Inorgánica e Instituto de Ciencia de Materiales de Sevilla, Universidad de Sevilla-C.S.I.C., Apdo. 874,41071-Sevilla, Spain

Received January 2, 1995; revised April 17, 1996; accepted April 18, 1996

The deactivation of Ni/SiO_2 catalysts by thiophene or H_2S during benzene hydrogenation at 200°C was studied as a function of the nickel reduction degree. An initial toxicity higher for thiophene than for H_2S was found at this relatively high temperature. Furthermore, the thiophene/H_2S toxicity ratio decreases on increasing the reduction degree of the sample. Temperature-programmed surface reaction (TPSR) results suggest that the difference in toxicity may be explained through a carbonaceous layer that remains adsorbed at 200°C on the nickel surface. TPSR results also revealed that thiophene is hydrogenolyzed to butane to a considerable extent on nickel surfaces at room temperature.

INTRODUCTION

Nickel catalysts used in hydrogenation, methanation, or steam-reforming reactions undergo strong deactivation when sulfur-containing compounds, H_2S, or organic compounds, such as thiophene, are present in the reactants stream (1–3). This poisoning is mainly dependent on the physicochemical properties of the catalyst (4–7), temperature, and the type of the sulfur compound (2, 8).

Duprez and Mendez (5), studying thiophene deactivation on Ni/Al_2O_3 catalysts, report that nickel thioresistance decreases on increasing the reduction degree of the metallic phase. Similar conclusions were reached for thiophene by Aguinaga *et al*. for Ni/SiO_2–Al_2O_3 and Ni/Al_2O_3 catalysts (7). These authors (5, 7) found that the presence of unreduced metal favors the thioresistance of nickel and consequently decreases the initial toxicity. These results can be explained by (i) the unreduced fraction of nickel acting as a sulfur trap for the poison, (ii) a combination of electronic effects ($Ni–Ni^{+2}$) and geometric effects, and (iii) dilution of the nickel surface by unreduced species.

For Ni/Al_2O_3 catalysts, Ahmed *et al*. (8) found that thiophene adsorption on nickel is structure sensitive in such a way that, on increasing the metal particle size, the Ni/C_4H_4S stoichiometry decreases from 0.39 for particles having a mean diameter of 3.3 nm to 0.23 for 9.2-nm mean diameter particles.

At low temperatures, the toxicity of sulfur compounds is influenced by their size and nature. Maxted (2), in a study of the toxicity of sulfur compounds on Ni and Pt catalysts in the 15–50°C range reported that the longer the hydrocarbon chain or molecule complexity, the higher the toxicity. However, at higher temperatures, complete hydrogenolysis of thiophene to butane and H_2S is thought to occur, H_2S being the actual sulfiding agent (9). Nevertheless, the temperature limit at which the complete hydrogenolysis occurs is not clearly stated. At 200°C, the S/Ni stoichiometry was found to be 0.25 by Bourne *et al*. (9) corresponding to a fully covered surface and admitting that sulfidation is confined to the surface. The stoichiometry found for sulfur adsorbed on Ni single crystals at saturation coverage is independent of the crystal face and equal to 0.58 (10). Mangnus *et al*. (11) postulate that at temperatures as high as 220°C sulfidation occurs in the inner layers with S/Ni_{sup} stoichiometries higher than one. Recently, in an EXAFS study of sulfided Ni catalysts, it has been demonstrated (12) that completely deactivated catalysts, using thiophene as poisoning agent, have surface layers that correspond to Ni_3S_2 phases. These discrepancies between monolayer capacity can be understood in several ways, (i) sulfur partially desorbs as H_2S in an H_2 atmosphere, which does not seem likely, (ii) thiophene remains adsorbed at such high temperatures, reducing the S/Ni stoichiometry, or (iii) cracking of the organic molecule occurs, resulting in carbonaceous fragments that also poison active metallic sites for hydrogenation. This latter hypothesis has found support in previous studies by HREELS, TDS, NEXAFS, and SEXAFS on the chemisorption of thiophene on Ni single crystals (13, 14).

In the present work, the hydrogenation of benzene to cyclohexane in the presence of H_2S or thiophene has been

[1] Current address: Departamento de Química Inorgánica e Instituto de Ciencia de Materiales de Sevilla, Universidad de Sevilla-C.S.I.C., Apdo. 874,41071-Sevilla, Spain.

[2] To whom correspondance should be addressed.

0021-9517/96 $18.00

studied at 200°C, as a function of the reduction degree of the Ni/SiO_2 catalyst. In this way, the influence of the unreduced phase on the thioresistance to sulfur compounds as well as on the hydrogenolysis behavior of thiophene at 200°C may be stated. A very different toxicity has been found for both poisons at such high temperature, which suggests that thiophene poisoning occurs via a complex mechanism. To clarify these differences, thiophene hydrogenolysis, using temperature-programmed surface reaction (TPSR) has been investigated.

EXPERIMENTAL

Catalyst: Ni/SiO_2. Catalysts were prepared by the precipitation–deposition method (15). Nickel, from an aqueous solution of nickel nitrate [80 g of $Ni(NO_3)_26H_2O$ (Merk, a.r. grade) in 2 liters of distilled water] slurried with silica [80 g of silica $100 < dp < 200$ μm (Kali Chemie AF125)] was precipitated onto the silica surface by a slow and homogeneous pH increase, produced by the thermal decomposition of urea [54 g/liter (Merck, a.r. grade)]. The slurry stirred at 90°C for 6 h. The sample was then dried at 110°C for 16 h and calcined in a 150 $cm^3/min/g_{cat}$ stream of air for 16 h at 500°C. After dissolving the catalyst in hydrofluoric acid, the nickel content was determined by AAS. After calcination treatment, the nickel content determined for the precursor was 15.5 w/w %, and the specific BET surface area 280 m^2/g.

Two series of catalysts were prepared by *in situ* reduction of the precursor. Prior to catalytic testing, the samples were reduced *in situ*, at 300, 350, 400, or 500°C in a 150 cm^3/min stream of hydrogen (heating rate 8°C/min) for 3 or 14 h for each temperature. Every sample was named indicating temperature and reduction time, i.e., the sample PD300,3 was reduced at 300°C for 3 h. The whole set of reduction treatments is presented in Table 1.

DRIFTS analysis. DRIFTS spectra were obtained in a Fourier transform Nicolet 5 DXC instrument (4000–400 cm^{-1}) in the diffuse reflectance mode. A catalytic chamber (Spectra Tech with KBr windows allows "*in situ*" treatments and analysis (RT, 875 K). The sample was placed in powdered form in the sample holder and the temperature monitored with a thermocouple located in physical contact with the sample. The resolution was 4 cm^{-1} and a satisfactory signal-to-noise ratio was obtained by accumulating 200 interferograms. To allow comparisons, the silica support was calcined at 500°C prior to DRIFTS measurements. Infrared spectroscopy studies of carbon monoxide adsorption were performed in the above experimental apparatus. After the reduction treatment, samples were flushed out under N_2 flow. The samples were then cooled to room temperature in flowing N_2 and a CO stream was mixed with the carrier ($P_{CO} < 5$ Torr) (1 Torr = 133.33 N/m). The spectrum of CO was directly computed from spectra recorded before CO adsorption and that obtained after N_2 flushing out CO excess.

Hydrogen chemisorption. H_2 chemisorption data were obtained at room temperature using the static method in an automatic volumetric apparatus (Micromeritics ASAP 2000C). The extent of reduction (f) was determined, after hydrogen chemisorption, by measuring the uptake of pure oxygen at 430°C. Both methods were conducted according to Ref. (16). Nickel particle diameters were calculated according to the method proposed by Coenen for this type of catalyst (17).

Catalytic reactions. Reactions were carried out in a differential fixed-bed reactor at 200°C and atmospheric pressure. The benzene (Fluka P.A.) was first treated with Raney nickel under reflux for 3 h and subsequently distilled. Benzene treated in this way was used in an attempt to check the degree of deactivation in the absence of thiophene, and no deactivation was found during a 6-h-long catalytic test. To prepare the sulfurized feedstock mixture, 5 ppm of thiophene was added to the purified benzene. The mixture was stored in two thermostated gas saturators. After reduction of the catalyst, the reactor was cooled to the reaction temperature in a flow of argon. The reaction mixture was obtained by passing a flow of hydrogen through the saturators thermostated at 10°C and kept at 1140 Torr by means of a pressure regulator [Brooks 5866]. The benzene and thiophene partial pressures were calculated assuming that the dilute (5 ppm) thiophene in benzene behaved as an ideal solution. To calculate the saturation pressures at the saturator temperature, Antoine's equations were used (18). Hydrogen (99.999%) was used throughout this work. Benzene conversions of less than 10% (differential reactor with respect to benzene) were obtained adjusting the weights of catalysts and the weight hourly space velocity. Reaction rate control by internal or external diffusion has been discarded in preliminary tests carried out using different catalyst particle sizes and different linear velocities at constant (W/F_{A0}),

TABLE 1

Nomenclature, Reduction Treatment, and Degree of Reduction of the Samples

Sample	Temperature (°C)	Time (h)	f^a (%)
PD300,3	300	3	1
PD350,3	350	3	10
PD400,3	400	3	53
PD500,3	500	3	90
PD300,14	300	14	5
PD350,14	350	14	42
PD400,14	400	14	78
PD500,14	500	14	89

[a] Degree of reduction.

respectively. H_2S deactivation tests were performed by mixing the stream of hydrogen/benzene coming from the saturators with a H_2S/H_2 calibrated mixture (10 ppm H_2S in H_2) resulting in a final H_2S concentration of 0.15 ppm. To avoid H_2S adsorption on the steel connecting tube, a Teflon tube was used for the H_2S/H_2 mixture. Likewise a Pyrex reactor was employed. The benzene to cyclohexane conversion was measured by on-line gas chromatographic analysis (Hewlett-Packard 5890) equipped with a TC detector. The conditions for the analysis were as follows: packed column 2.5% CW-20M on DMCS 80/100, injector temperature l50°C, oven temperature 80°C, detector temperature 150°C, carrier gas hydrogen, 30 cm^3/min.

Temperature-programmed surface reaction. TPSR tests were carried out after 25 or 200°C thiophene saturation (in a thiophene in argon stream) of the previously reduced catalyst. Samples saturated at 200°C were cooled in Ar to room temperature and the excess thiophene was then flushed out with hydrogen at 25°C. The samples were heated 5 min^{-1}) in flowing hydrogen (50 cm^3/min), and the product yields were determined by on-line gas chromatography. The conditions for the analysis were: packed column SP/700 + BMEA on CHROMP-AW, injector and detector temperature 150°C, oven temperature 100°C, and carrier gas hydrogen, 30 cm^3/min.

Catalyst sulfur content. The sulfur content of the samples was determined after TPSR with an ANTEK 701 C fluorescence sulfur system.

Catalyst carbon analysis. The carbon deposit of the samples was determined after the TPSR test with a CS-244 LECO instrument.

RESULTS AND DISCUSSION

The X-ray diffraction pattern of the oxidized precursor catalysts showed poorly defined XRD peaks, which are usually associated with nickel antigorite-like domains (19, 20). Peaks due to NiO are absent in the X-ray pattern, suggesting that nickel is present in the form of the nickel antigorite interaction compound.

TPR profiles, not presented here, are characterized by a broad peak extending up to 800°C with a maximum at around 600°C. The similarity with previous data for Ni/SiO_2 samples prepared by this method (21) confirms the existence of an interaction compound. The broad temperature range for the catalyst reduction allows a series of catalysts with different reduction degrees to be obtained by means of the systematic change in the reduction treatment (Table 1).

Hydrogen chemisorption data obtained by the static method are shown in Table 2. It can be seen that on increasing the temperature and time of reduction, the total amount of adsorbed hydrogen increases. The percentage of reversible hydrogen adsorbed also increases on decreasing the reduction degree of the sample. The table also includes the metallic dispersion (D) calculated as the percentage of exposed Ni atoms per total number of Ni atoms ($Ni^0 + Ni^{2+}$), the average particle size for nickel (d), and the number of accessible Ni atoms per gram of catalysts. This latter calculation has been carried out using the irreversible hydrogen adsorption for PD300,14 and PD300,3 catalysts. For all the other catalysts the total amount of adsorbed H_2 was used. This criteria were taken from Anderson and Pratt (22). These authors proposed the use of the total volume of adsorbed hydrogen for particle sizes higher than 1 nm; for particle sizes below 1 nm they recommend the use of the irreversible volume of adsorbed hydrogen. For the samples reduced at 300°C the calculated metallic dispersion, using the total amount of adsorbed hydrogen (data in brackets), was higher than 100%. This result is in good agreement with the stoichiometry proposed by Anderson and Pratt (22). Similar results were obtained by Sayari *et al.* (23) for a ruthenium catalyst. The particle sizes deduced from H_2 chemisorption were confirmed by TEM.

TABLE 2

Hydrogen Chemisorption Data of the Catalyst after Different Reduction Treatments

Sample	H_2 total (STP cm^3/g_{cat})	H_2 irrev (STP cm^3/g_{cat})	H_2 rev/H_2 total (%)	D^a (%)	d^b (nm)	At $Ni_{acc}/g_{cat}{}^d$ ($\times 10^{-20}$)
PD300,3	0.38	0.20	47.4	66.2 (127[c])	1.0	0.10
PD350,3	1.91	1.00	47.6	64.7	1.0	1.03
PD400,3	3.43	2.08	39.4	21.9	3.0	1.84
PD500,3	8.37	5.52	34.1	31.4	2.1	4.49
PD300,14	2.30	1.18	48.7	79.6 (155[c])	0.8	0.63
PD350,14	3.28	1.87	43.0	26.4	2.5	1.77
PD400,14	7.98	5.43	32.0	34.5	1.9	4.29
PD500,14	8.16	5.83	28.6	31.0	2.1	4.39

[a] Metallic dispersion (exposed Ni atoms/total Ni content of the sample).
[b] Average nickel particle size.
[c] Between brackets, dispersion percentage calculated using the total hydrogen adsorbed.
[d] Number of accessible Ni atoms per gram of catalysts.

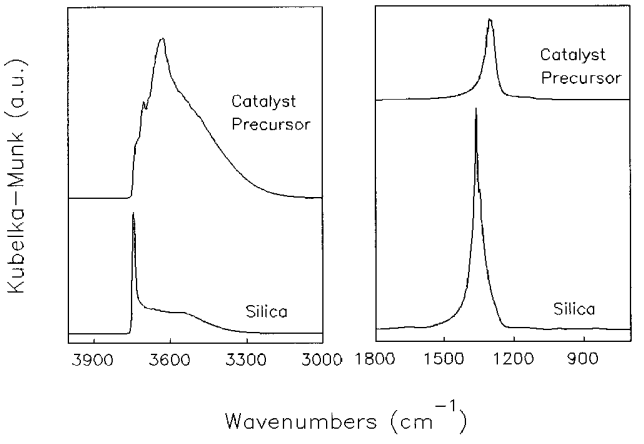

FIG. 1. DRIFTS spectra of the support, silica, and the catalyst precursor.

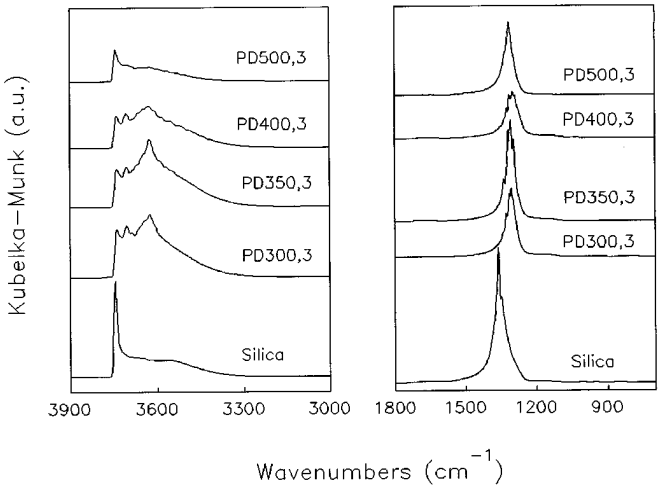

FIG. 2. DRIFTS spectra of the support, silica, and the catalyst after different reduction treatments.

Figure 1 shows the DRIFTS spectra of the silica support, air calcined at 500°C, and the catalyst precursor in the 3900–3000 cm^{-1} and 1800–700 cm^{-1} ranges. The main absorption band peaking at 1360 cm^{-1} has been ascribed to transverse (TO) and longitudinal (LO) optical modes of the silica support (24, 25). This band shifts to lower wavenumbers on the nickel/silica sample. Capitán *et al.* (26) found a similar shift for the Al–O stretching frequency in Ln_2O_3/γ-Al_2O_3 systems on supporting the oxide phase. A second neighboring influence through the formation of Ln–O–Al bonds has been pointed out as responsible for such a shift. The DRIFTS spectrum, in the OH stretching region, of the catalyst precursor also shows important modifications with respect to the support. The sharp and intense band at 3749 cm^{-1} present in the support is replaced in the precursor by a less intense band, at the same frequency. In addition, bands at 3700 and 3625 cm^{-1}, as well as a broad and featureless band at around 3500 cm^{-1}, appear. Both, the Si–O stretching frequency shift and the OH stretching modification are in agreement with the formation of an antigorite-like phase on the support surface as previously described for precipitation–deposition Ni/SiO_2 precursors (27).

On reducing the precursor, the OH stretching region is modified as a function of the reduction treatment, Fig. 2. As the reduced nickel fraction increases, the OH features ascribed to hydroxysilicate phases, peaks at 3700 and 3625 cm^{-1}, decrease in intensity corresponding to the elimination of Ni^{2+} species. For the more reduced sample, the OH spectrum is similar to the one obtained for the support, except for a lower intensity of the 3749 cm^{-1} peak, which indicates that NiO particles are built over an interface made of nickel hydroxysilicate, this being confirmed by the stretching frequency of the Si–O bonds that remains almost unaltered with respect to the catalyst precursor. This structure of the Ni/SiO_2 catalyst prepared by the precipitation–deposition method is in agreement with that proposed by Coenen (17).

As stated above, the effect of the reduction degree on the thioresistance of nickel catalysts is related by some authors (5, 7) to electronic effects derived from the Ni^{2+}–Ni^0 interface. CO chemisorption can be envisaged as an excellent tool for discerning electronic effects, since, π-backbonding of CO to the metallic surface is affected by the electron density of the active site (8). Hence, to identify possible electronic effects as a function of the reduction degree, CO chemisorption was studied by DRIFTS. Figure 3 shows the normalized spectra of CO irreversibly adsorbed at room temperature on the PD300,3; PD350,3; PD400,3; and PD500,3 catalysts.

According to literature data (29–32), absorption bands above 2000 cm^{-1} must be ascribed to stretching vibrations

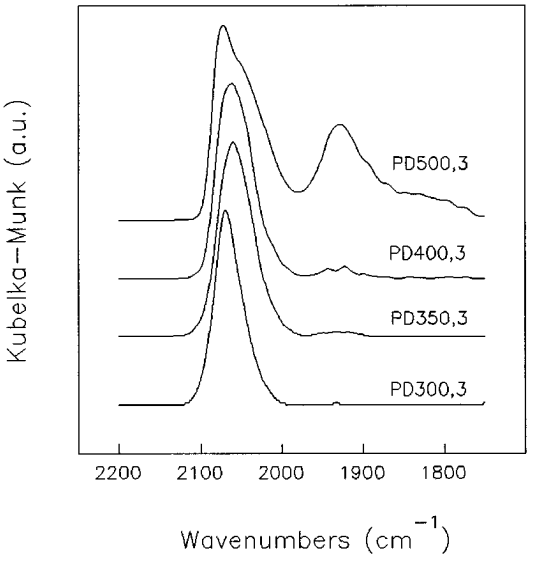

FIG. 3. Normalized DRIFTS spectra of CO adsorbed on the reduced samples at 25°C.

of linearly bonded CO, while bands below this frequency are due to bridged and multibonded species. The relative intensity of the band at 2070 cm^{-1}, with respect to the one at 2040 cm^{-1}, increases on decreasing the reduction degree. Several hypotheses may account for this fact: (i) electronic effects, in the system Ni^0/Ni^{2+}, Ni is expected to donate electrons to Ni^{2+} in order to equilibrate Fermi levels at the interface or (ii) an increase in the Ni particle size.

According to the (σ,π) bands scheme for CO chemisorption (33), the backdonation of Ni electrons to the πCO orbitals decreases, which results in a shift to higher wavenumbers of the CO stretching frequency. Thus, for incompletely reduced samples, the band position should be shifted to higher frequencies. Primet *et al.* (29) reported in detail the relative intensity change in a Ni/SiO_2 catalyst. These authors ruled out the electronic effect, since the presence of the electronic effect would lead to a continuous shift of the frequencies, whereas actually the two bands remain roughly at the same position. However, they suggest that the 2070 cm^{-1} band may be assigned to CO molecules linearly bonded to metallic nickel atoms in interaction with an oxide phase (unreduced nickel or silica), whereas the 2040 cm^{-1} band would correspond to CO linearly bonded to unperturbed nickel atoms. Blackmond and Ko (31) correlated the relative intensity of bands at 2040 and 2080 cm^{-1} with the mean particle size. Their results showed an increase in the relative intensity for the 2040 cm^{-1} band on increasing the mean particle size from 2.5 to 9 nm. The explanation of both Primet *et al.* (29) and Blackmond and Ko (31) are essentially similar since on increasing the particle size, a decrease in the Ni^0/Ni^{+2} or/and Ni/SiO_2 interfaces should be expected. Our data are consistent with these suggestions, since increases in both particle size and reduction degree (Table 2) are observed on going from PD300,3 to PD500,3 catalysts.

Similarly, the higher intensity of the bands at 1930 cm^{-1} (bridged carbonyl species) and 1810 cm^{-1} ($Ni_x(CO)$ with $x > 2$) (32) on increasing the reduction degree are consistent with an increase of higher symmetry sites on increasing the particle size.

Figure 4 shows the catalytic activity defined as the ratio of the reaction rate in the hydrogenation of benzene measured at a given time for PD500,14 ($f = 0.89$) and PD300,4 ($f = 0.05$) catalysts, poisoned with thiophene and H_2S, respectively, to that of the fresh catalyst. Defining the initial toxicity as the number of Ni atoms at the catalyst surface that are deactivated by the first molecule of poison entering the reactor (34) and estimating it from the slope at the intercept of the activity vs the total amount of poison molecules per surface nickel atom curve (35), it is clear that thiophene is more toxic than H_2S.

Table 3 shows the initial toxicity for H_2S (T_{SH}) and thiophene (T_{TH}) for each catalyst. From the data in Table 3, it can be stated that, on increasing the reduction degree, the toxicity for both H_2S and thiophene increases, as previously

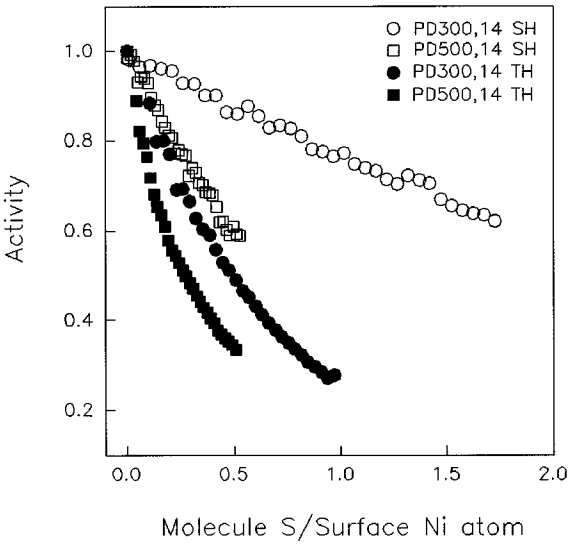

FIG. 4. Normalized catalyst activity as a function of the amount of sulfur fed into the reactor for the catalysts PD300,14 and PD500,14.

reported (5, 7). Moreover, whatever the reduction degree, the initial toxicity for thiophene is higher than that for H_2S. If the sulfiding mechanism for thiophene were related to the formation of H_2S and gaseous C_4H_{10} (9), the toxicity for both H_2S and thiophene should be the same. However, the thiophene/H_2S toxicity ratio is always higher than 1.0, depending on the reduction degree of the catalysts in such a way that, on increasing the reduction degree, the T_{TH}/T_{SH} ratio decreases (Fig. 5).

To clarify these differences in toxicity, TPSR experiments were carried out over H_2-reduced catalyst. Figure 6 shows the evolution of the eluted products as a function of temperature after thiophene saturation at 25°C for PD300,14; PD350,14; PD400,14; and PD500,14 catalysts. Products eluted can arise both from species produced during thiophene saturation and from species generated by the temperature program during TPSR, it being impossible to differenciate between these hypotheses in our experiments.

TABLE 3

Turnover Number (TON), Initial Toxicity H_2S (T_{SH}), and Thiophene (T_{TH}) on the Catalyst after Different Reduction Treatments

Sample	TON (s^{-1})	T_{SH}	T_{TH}
PD300,3	7.14	0.20	0.28
PD350,3	2.29	0.25	1.49
PD400,3	1.35	0.34	1.91
PD500,3	0.66	1.31	4.40
PD300,14	2.50	0.24	1.41
PD350,14	1.16	0.44	2.32
PD400,14	0.82	0.67	3.08
PD500,14	0.93	1.00	3.20

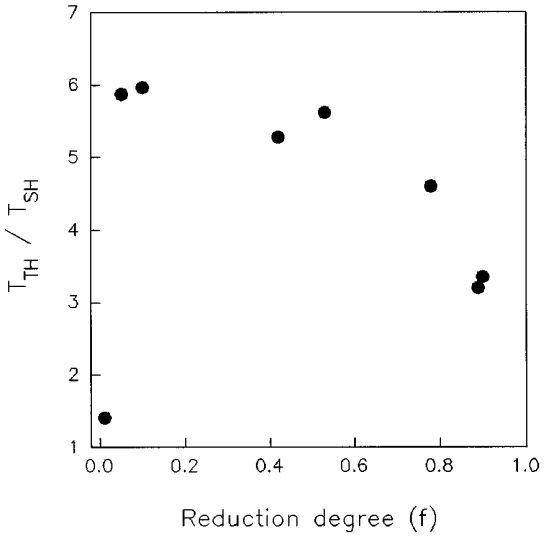

FIG. 5. Effect of the reduction degree of the nickel on the thiophene/H_2S initial toxicity ratio.

In general the TPSR patterns are dominated by a sharp peak corresponding to C_4H_{10} desorption at low temperatures, around 100°C, and complex profiles corresponding to CH_4 and C_3H_8 extending their evolution range up to temperatures well above 200°C.

The reduction temperature affects the TPSR pattern in several ways. The temperature at which the maximum desorption rate for butane occurs decreases on increasing the reduction degree, shifting from 150°C for the PD300,14 catalyst to 79°C for PD500,14 and PD400,14. Furthermore, a shoulder is evident at low temperatures for the less reduced catalyst. Methane and propane production increase

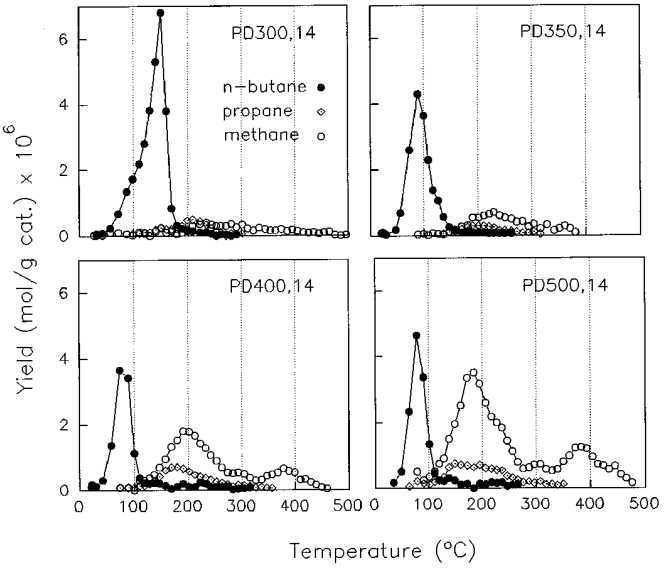

FIG. 6. Temperature-programmed hydrogenation products obtained after thiophene adsorption at 25°C.

TABLE 4

Amount of Sulfur Retained by the Catalysts after the TPSR Experiments

Sample	Saturation temperature (°C)	S_R[a] (mg S/g_{cat})	S_{TPSR}[b] (mg S/g_{cat})	S_{TPSR}/S_R (%)
PD300,14	25	2.60	2.28	87.7
PD350,14	25	3.54	1.47	41.5
PD400,14	25	5.25	1.58	30.1
PD500,14	25	8.29	2.17	26.2
PDAr500[c]	25	1.66	1.64	98.8
PD300,14	200	2.21	1.18	53.4
PD500,14	200	11.99	4.67	38.9

[a] Retained sulfur determined by analysis in the deactivated catalyst.
[b] Retained sulfur calculated from TPSR peaks integration.
[c] Unreduced catalyst precursor.

on increasing the fraction of reduced metal. The methane pattern is dominated by two peaks at around 200 and 400°C, the peak position shifting to lower temperatures for the more reduced catalysts. A similar effect is observed for propane profiles, although desorption of this product stops at slightly lower temperatures than that for methane.

By integrating the TPSR peaks areas and considering the stoichiometries

$$SC_4H_8 + 2H_2 \rightarrow H_2S + C_4H_{10}$$
$$SC_4H_8 + 3H_2 \rightarrow H_2S + C_3H_8 + CH_4$$
$$SC_4H_8 + 5H_2 \rightarrow H_2S + 4CH_4$$

the amount of thiophene hydrogenolyzed during the TPSR experiment can be calculated. This quantity is indicated in Table 4 as milligrams of sulfur per gram of catalyst (S_{TPSR}). Two main observations can be pointed out. First, the amount of hydrogenolyzed thiophene does not follow a simple pattern with respect to the reduction degree (Fig. 7). Second, it can be seen that the amount of thiophene hydrogenolyzed to butane decreased in a systematic way while the amount of propane and methane increased on increasing the reduction degree (Fig. 7). On the other hand, as shown in Fig. 6, the temperature of the peak for butane evolution decreases on increasing the reduction degree. Furthermore, for the less-reduced catalysts, a low-temperature shoulder is evident, while for the intermediate reduction degrees the shoulder is clearly observable at high temperatures. On this basis, two pathways can be postulated for hydrogenolyzing thiophene to butane, one sulfiding metallic Ni sites and the other Ni^{2+} cations. To check this hypothesis, TPSR experiments with a completely unreduced sample were carried out. Figure 8 presents the pattern of eluted products after RT adsorption of thiophene on the catalyst precursor. Most of the adsorbed thiophene evolves as C_4H_{10} at low temperatures, with a maximum evolution rate at 150°C, demonstrating that thiophene can be retained

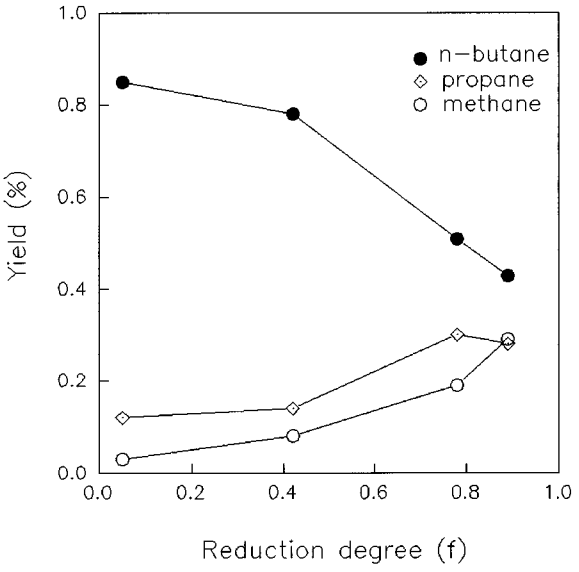

FIG. 7. Effect of the reduction degree of the nickel on the percentage of cracking products.

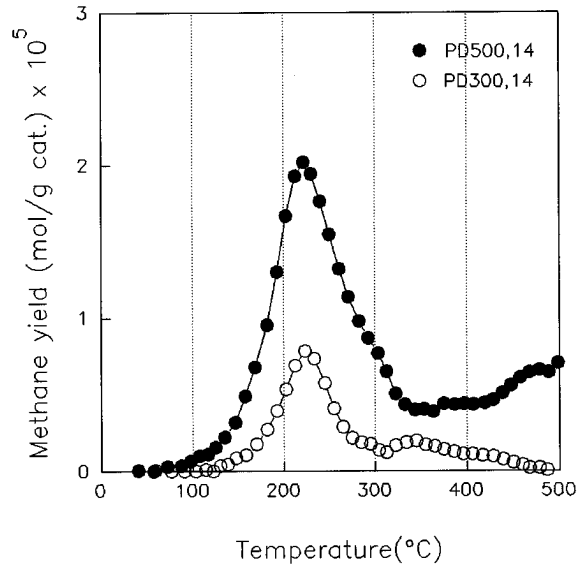

FIG. 9. Temperature-programmed hydrogenation spectra of adsorbed thiophene at 200°C on PD300,14 and PD500,14 catalysts.

and hydrogenolyzed on unreduced Ni phases. This was confirmed by sulfur analysis at the end of the experiment (Table 4). In addition, the maximum position coincides with the maximum observed in the less reduced sample, PD300,14. The interpretation of the rest of the products obtained above 250°C is not easy, since during the TPSR processes nickel could be reduced from this temperature, although cracking of SC_4H_8 cannot be disregarded.

Figure 9 shows the evolving profiles after thiophene saturation at 200°C. In this case, methane is the only product found, with a maximum at 210°C, and is still evolving at temperatures higher than 500°C.

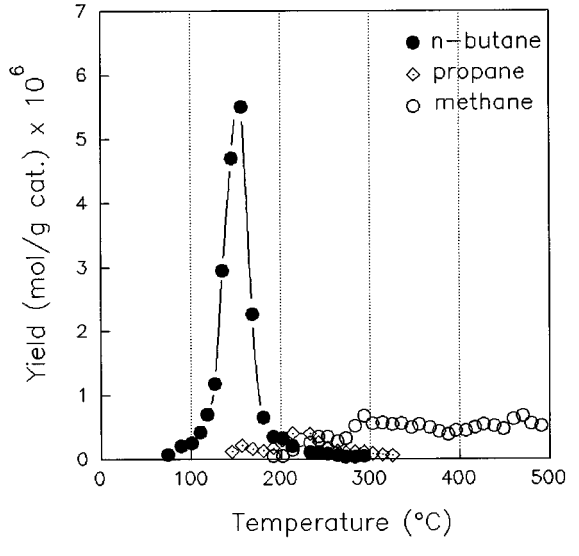

FIG. 8. Temperature-programmed hydrogenation spectra of adsorbed thiophene at 25°C on the unreduced catalyst precursor.

From these results, two hypotheses can be postulated. In the first, the formation of three different TPSR products could be explained in terms of thiophene hydrogenolysis products derived from three different configurations of adsorbed thiophene on the nickel surface. As has been discussed in the literature (36, 37), the orientation of the thiophene ring with respect to the surface is of importance in determining the decomposition pathway. The second hypothesis supposes the rupture of the S–C bond, resulting in a carbonaceous deposit that is further dehydrogenated/hydrogenated. From this latter hypothesis, the TPSR methane pattern obtained resembles the one for temperature-programmed hydrogenation (TPH) spectra of carbon deposits described by Chen and Chen (38) on 15% Ni/Al_2O_3 catalyst. These authors found three TPH peaks (noted as low-, intermediate-, and high-temperature peaks) ascribed to three types of surface carbon.

The evolution of TPSR products observed in Figs. 6 and 9 at temperatures clearly higher than the deactivation test temperature (200°C) suggests that thiophene or a carbonaceous residue remains adsorbed on the nickel surface at this temperature.

To quantitatively check our results, the amount of sulfur retained (S_R) determined in the deactivated catalyst after the TPSR experiments was compared with the amount of sulfur resulting from the integration of the TPSR peaks (S_{TPSR}) shown in Figs. 6 to 9 and taking into account the appropriate stoichiometric relations. These results are presented in Table 4, in which it can be observed that the calculated sulfur amount only accounts for a fraction of the total sulfur content, the discrepancy being larger for the more reduced catalysts. In an attempt to explain these discrepancies, the following two hypotheses may be considered:

(i) The upper limit of TPSR experiments was set to 500°C. However, it is possible that, at this temperature, thiophene or some carbonaceous species arising from it, remained adsorbed on the catalyst, thus reducing the calculated sulfur amount.

(ii) The experimental setup does not permit routine analysis of the gas stream coming from the reactor during thiophene saturation or while flushing out thiophene excess with H_2 at 25°C. If thiophene is hydrogenolyzed during these procedures, then the corresponding amount of retained sulfur will not be computed by integration of the TPSR peaks. Although according to Abmed *et al.* (8), thiophene should be not hydrogenolyzed over nickel catalysts at room temperature, a TPSR experiment was designed to test this statement, to allow us to carry out some analysis of the H_2 flushing out thiophene excess at 25°C. Although an accurate quantification of the evolved gases was not possible, due to the minimum time between analysis and the sharpness of the elution peak, an intense butane peak was detected at the beginning of the flushing-out period (Fig. 10). This result clearly demonstrates that thiophene is hydrogenolyzed over nickel catalysts at room temperature, and the discrepancies observed in Table 4 between S_R and S_{TPSR} are mainly associated to room temperature hydrogenolysis of thiophene. However, it should be also noted that methane evolution (Fig. 6) is not complete at temperatures as high as 500°C. Thus both room-temperature hydrogenolysis of thiophene and the remaining carbon on the catalysts surface account for the discrepancies in Table 4. It is clear that complete hydrogenolysis of thiophene does not occur at 200°C, the deactivation temperature chosen in this work.

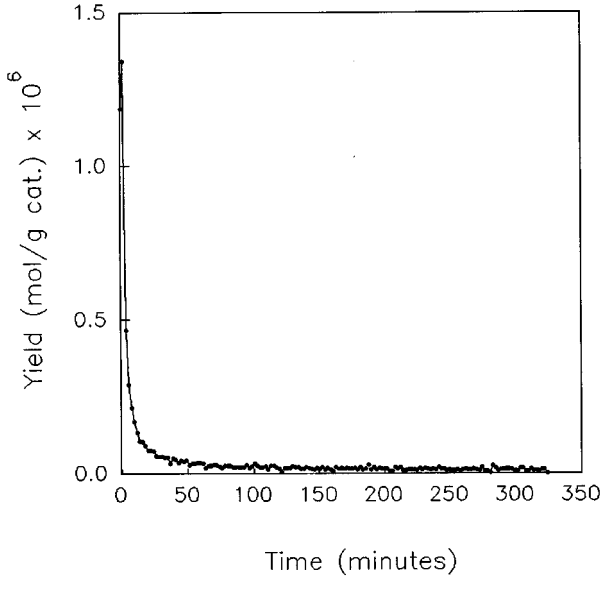

FIG. 10. *n*-Butane elution curve during H_2 purging at 25°C after saturation of PD500,14 sample at room temperature.

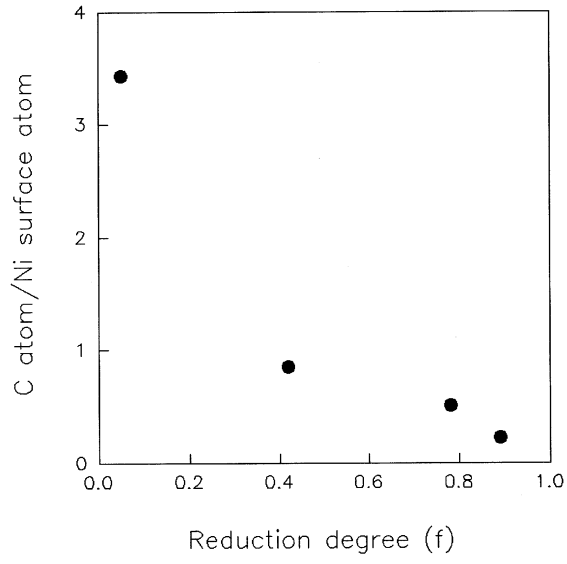

FIG. 11. Effect of the reduction degree of the nickel on the carbon atoms deposited per nickel surface atom.

The amount of carbon remaining in the catalysts in the adsorbed residue was analyzed. Figure 11 shows the results obtained for the samples after TPSR experiments, expressed as the number of carbon atoms referred to the number of accessible Ni atoms. This analysis confirms carbon deposition as a result of thiophene C–S breaking and subsequent dehydrogenation. It must be pointed out that no deactivation was found for a 6-h-long catalytic test in the absence of thiophene, ruling out the benzene origin of the carbonaceous deposit.

In addition to this, it can be stated that the higher the reduction degree, the lower the amount of retained carbon. This fact would be in good agreement with the very strong propensity of metallic nickel to cause complete hydrocracking of hydrocarbons to methane (38).

EVALUATION

Sulfur analysis after TPSR tests on unreduced samples have confirmed the capacity of the unreduced nickel fraction for retaining sulfur. Hence, the unreduced fraction may act as a sulfur trap for the poisoning molecules, although the contribution of the interphase Ni^0–Ni^{2+} cannot be disregarded. The DRIFTS spectra of irreversibly adsorbed CO, Fig. 3, show the important presence of such an interphase, through the presence of the 2070 cm^{-1} band.

Oudar (3), studying changes in the work function, found that sulfur chemisorption on nickel, at monolayer coverage, generates a slight electron transfer toward the sulfur atom. On the basis of LEED data, this author studied the covalent nature of the S–Ni bond, stating that the electronic transfer can modify this bond. The presence of Ni^{2+} could decrease the electronic density of Ni, and the nickel particles

would have a deficient electronic character. On this bases, the electron-deficient character of Ni sites would improve the sulfur resistance. This is in agreement with the results reported by Sauvion *et al.* (39), who studied the resistance of Ni/Support catalyst containing Ce^{4+} and Ce^{3+} to poisoning by H_2S during butane hydrogenolysis. They found that Ce^{4+}, which improved the electron-deficient character at the Ni, increased the sulfur resistance of the catalysts. A similar effect has been found by Duprez and Mendez for Ni/Al_2O_3 catalysts (5). These authors reported that the presence of unreduced nickel improved the thioresistance of nickel.

The influence of the metallic particle size on the electronic effect has been widely studied (6, 40, 41). In these works, the structure sensitivity of sulfur adsorption on metallic surface has been determined. However, it must be pointed out that, in metallic-supported particles, is not easy to discriminate between the particle size electronic effect and the electronic effect produced by the support–metal interaction (42). In addition, the electronic character of the nickel particles improves the hydrogenolysis of the thiophene molecule. Somorjai (43) postulated that the atoms of the faces were more efficient for C–C bond breaking while the atoms of the corner and edges showed more activity from the C–H and H–H bond breaking.

The H_2 chemisorption measurements show the increase of the reversible hydrogen percentage adsorbed on decreasing the reduction degree. Hydrogen reversibly adsorbed has been previously attributed to chemisorption sites at the metal-unreduced phase interface or to metallic sites with a deficiency of electrons (44–47). Therefore, these chemisorption results are also in agreement with the relative extent metal-unreduced phase interface as a function of the reduction degree.

However, electronic effects have to be ruled out due to CO chemisorption data. The presence of the electronic effects would lead to a continuous shift of CO stretching frequencies and our results clearly demonstrate that bands remain at the same position, whatever the reduction degree of the catalyst.

The metal-unreduced phase interface should show a maximum as a function of the reduction degree as a result of the combination of two synergetic effects: the particle size and the amount of unreduced phase.

It is clear, however, that the unreduced phase may retain sulfur (Table 4), in this case, considering that the thioresistance is calculated from an estimate to the number of metallic surface nickel atoms. As a consequence, all the sulfur atoms held by the unreduced phase result in a toxicity estimation below the one calculated in the absence of the unreduced phase.

Results in Table 3 indicate that, whatever the reduction degree, the initial toxicity for thiophene is higher than that for H_2S. It is accepted in the literature that the influence of the size and nature of sulfur compounds influence their toxicity to metallic sites at low temperatures. However, at 200°C, different authors (9, 48) reported a complete hydrogenolysis of thiophene to butane and H_2S. The results of deactivation presented in this work have been obtained at 200°C, so the higher toxicity observed from thiophene molecules cannot be explained by this model.

The evolution of TPSR products observed at temperatures clearly higher than the deactivation test (200°C) and the carbon analysis after the TPSR experiment suggest that a carbonaceous layer remains adsorbed at this temperature on the nickel surface. The higher Ni/S stoichiometry of the proposed adsorbed thiophene configurations with respect to H_2S, as presented above, is also in agreement with the higher toxicity found for this molecule on nickel at 200°C. This fact seems to be in agreement with the results shown in Fig. 9, in which methane evolution is detected after thiophene saturation at 200°C, thus proving that thiophene or carbonaceous moieties from it can remain adsorbed at the deactivation temperature used in this work. On the other hand it has been found (Fig. 5) that the thiophene/H_2S toxicity ratio increases on decreasing the metallic nickel at the surface. In relation to this, carbon deposit analysis indicates that the hydrogenation and subsequent removal of the carbon fragments at the surface would be improved for the more reduced catalyst.

CONCLUSIONS

The initial toxicity of thiophene and H_2S decreases on decreasing the reduction degree, and this behavior has been mainly explained as a trap effect by the unreduced fraction of nickel. It has been stated that thiophene is hydrogenolyzed to an important extent on Ni a 25°C as demonstrated by the fact that TPSR products have been detected at this temperature.

The evolution of TPSR products observed at temperatures higher than that of the deactivation test (200°C) and carbon analysis indicate that carbonaceous species adsorbed at the reaction temperature are present, explaining the higher toxicity found for the thiophene molecule. However, it must be pointed out that carbon fragments removal is promoted by the increase of the reduced fraction of the nickel.

ACKNOWLEDGMENTS

The financial support by the Excelentísima Diputación Foral de Guipuzcoa is gratefully appreciated. In addition, we thank A. Uceda from Leco Instrumentos S.A. for performing the carbon analyses.

REFERENCES

1. Bartholomew, C. H., Agrawal, P. K., and Katzer, J. R., *Adv. Catal.* **31**, 135 (1982).
2. Maxted, E. B., *Adv. Catal.* **3**, 129 (1951).

3. Oudar, J., *Catal. Rev.-Sci. Eng.* **22**, 171 (1980).
4. Del Angel, G., Coq, R., Figueras, F., Fuentes, S., and Gomez, R., *in* "Proceedings, 8th Simposio Iberoamericano de Catálisis," Vol. 1, p. 180. La Rábida, 1982.
5. Duprez, D., and Mendez, M., *in* "Catalyst Deactivation" (B. Delmon and G. F. Froment, Eds.), p. 523. Elsevier, Amsterdam, 1987.
6. Guenin, M., Breysse, M., Fretty, R., Tifouty, K., Marecot, P., and Barbier, J., *J. Catal.* **105**, 144 (1987).
7. Aguinaga, A., Montes, M., and Asua, J. M., *J. Chem. Tech. Biotechnol.* **52**, 369 (1991).
8. Ahmed, K., Chadwick, D., and Kershembaum, L. S., *in* "Catalyst Deactivation" (B. Delmon and G. F. Froment, Eds.), p. 513. Elsevier, Amsterdam, 1987.
9. Bourne, K. H., Holmes, P. D., and Pickethcy, R. C., *in* "Proceedings, 3rd International Congress on Catalysis, Amsterdam, 1964" (W. M. H. Sachtler, G. C. A. Schuit, and P. Zwietering, Eds.), p. 1401. Wiley, New York, 1965.
10. Perdereau, M., and Oudar, J., *Surf. Sci.* **20**, 80 (1970).
11. Mangnus, P. J., Poels, E. K., Van Langeveld, A. D., and Moulijn, J. A., *J. Catal.* **137**, 92 (1992).
12. Aguinaga, A., Montes, M., Malet, P., Capitán, M. J., Carrizosa, I., and Odriozola, J. A., *Appl. Catal. A: General* **110**, 197 (1994).
13. Stohr, J., Kollin, E. B., Fischer, D. A., Hastings, J. B., Zaera, F., and Sette, F., *Phys. Rev. Lett.* **55**, 1468 (1985).
14. Zaera, F., Kollin, E. B., and Gland, J. L., *Langmuir* **3**, 555 (1987).
15. Van Dillen, J. A., Geus, J. W., Hermans, L. A. M., and Van der Meigden, J., *in* "Proceedings, 6th International Congress on Catalysis, London, 1976" (G. C. Bond, P. B. Wells, and F. C. Tompkins, Eds.), p. 477. The Chemical Society, London, 1977.
16. Bartholomew, C. H., and Farrauto, R. J., *J. Catal.* **45**, 41 (1976).
17. Coenen, J. W. E., *Ind. Eng. Chem. Fundam.* **25**, 43 (1986).
18. Reid, R. C., Prausnitz, J. M., and Poiling, B. E., *in* "The Properties of Gases and Liquids," N4. McGraw-Hill, New York, 1988.
19. Montes, M., Penneman de Bosscheyde, C., Hodnett, B. K., Delannay, F., Grange, P., and Delmon, B., *Appl. Catal.* **12**, 304 (1984).
20. Coenen, J. W. E., and Linsen, B. G., *in* "Physical and Chemical Aspects of Adsorbens and Catalysts" (B. G. Linsen, Ed.), p. 495. Academic Press, London, 1970.
21. Gil, A., Díaz, A., Gandía, L. M., and Montes, M., *Appl. Catal. A: General* **109**, 167 (1994).
22. Anderson, J. R., and Pratt, K. C., "Introduction to Characterization and Testing of Catalyst," Academic Press, North Ryde, Australia, 1985.
23. Sayari, A., Wang, H. T., and Goodwin, Jr., J. G., *J. Catal.* **93**, 368 (1985).
24. Benzinger, J. B., McGovern, S. G., and Royce, B. S. H., *in* "Catalyst Characterization Science: Surface and Solid State Chemistry" (M. L. Deviney and J. L. Gland, Eds.), Vol. 288, p. 449. ACS Symposium Series. Am. Chem. Soc., Washington, DC, 1985.
25. Scott, J. R., and Porto, S. P., *Phys. Rev.* **161**, 903 (1967).
26. Capitán, M. J., Centeno, M. A., Malet, P., Carrizosa, I., Odriozola, J. A., Márquez, A., and Fernández Sanz, J., *J. Phys. Chem.* **99**, 4655 (1995).
27. Ghuge, K. D., Bhat, A. N., and Babu, G. P., *Appl. Catal. A: General* **103**, 83 (1993).
28. Doyen, G., and Erlt, G., *Surf. Sci.* **43**, 197 (1974).
29. Primet, M., Dalmon, J. A., and Martin, G. A., *J. Catal.* **46**, 25 (1977).
30. Rochester, C. H., and Terrell, R. J., *J. Chem. Faraday Trans. 1* **73**, 609 (1977).
31. Blackmond, D. B., and Ko, E. I., *J. Catal.* **96**, 210 (1985).
32. Sheppard, N., and Nguyen, T. T., *in* "Advances in Infrared and Raman Spectroscopy" (P. J. Clarke and R. E. Hester, Eds.), Vol. 5, p. 67. Wiley, New York, 1978.
33. Blyholder, G., *J. Phys. Chem.* **68**, 2722 (1964).
34. Barbier, J., *in* "Deactivation and Poisoning of Catalyst" (J. Oudar and H. Wise, Eds.), p. l09. Dekker, New York, 1985.
35. Aguinaga, A., Montes, M., de la Cal, J. C., and Asua, J. M., *Ind. Eng. Chem. Res.* **31**, 155 (1992).
36. Kelly, D. G., Salmeron, M., and Somorjai, G. A., *Surf. Sci.* **175**, 465 (1986).
37. Zaera, F., Kollin, E. B., and Gland, J. L., *Surf. Sci.* **184**, 75 (1987).
38. Chen, I., and Chen, F., *Ind. Eng. Chem. Res.* **29**, 534 (1990).
39. Sauvion, G. N., Akalay, I., Guilleux, M. F., Tempere, J. F., and Delafasse, D., *J. Chim. Phys.* **80**, 769 (1983).
40. Gazellot, P., Datka, J., Massardier, J., Primet, M., and Imelik, B., *in* "Proceedings, 6th International Congress on Catalysis, London, 1976" (G. C. Bond, P. B. Wells, and F. C. Tompkins, Eds.), p. A 11. The Chemical Society, London, 1977.
41. Biswas, J., Bickle, G. M., Gray, P. G., and Do, D. D., *in* "Catalyst Deactivation" (B. Delmon and G. F. Froment, Eds.), p. 553. Elsevier, Amsterdam, 1987.
42. Barbier, J., Lamy-Pitara, E., Marecot, P., Boitiaux, J. P., Cosyns, J., and Verna, F., *in* "Advances in Catalysis" (D. D. Eley, H. Pines, and P. B. Weisz, Eds.), Vol. 37, p. 279. Academic Press, San Diego, 1991.
43. Somorjai, G. A., *Adv. Catal.* **26**, 2 (1977).
44. Rankin, J. L., and Bartholomew, C. H., *J. Catal.* **100**, 533 (1986).
45. Revel, R. C., and Bartholomew, C. H., *J. Catal.* **85**, 63 (1984).
46. Hardeveld, R., and Hartog, F., *Surf. Sci.* **15**, 189 (1969).
47. Slinken, A. A., Kucherov, A. V., and Rubinsheim, A. M., *Kinet. Catal.* **19**, 415 (1978).
48. Klostermann, K., and Hobert, H., *J. Catal.* **63**, 355 (1980).